Analyses of Beamspace MIMO Channels at 142 GHz

Mar Francis De Guzman, Nuutti Tervo, *Member, IEEE*, Pekka Kyösti, *Member, IEEE*, and Katsuyuki Haneda, *Member, IEEE*

***Abstract*—This letter presents the analyses of a single-user beamspace multiple-input–multiple-output (MIMO) on measured indoor and outdoor channels at 142 GHz. The rank is evaluated under different antenna sizes, number of beams, and thresholds. We assume a total power constraint at the transmitter that results in a decrease in a signal-to-noise ratio as the link distance increases. When using spatial multiplexing, the indoor and outdoor sites demonstrate an average capacity gain of 2× and 1.5× at link distances below 60 m. Also, the rank for our measured 142 GHz channels is comparable to that at 60 GHz channels but significantly lower than the rank at 5 GHz channels reported in the literature. We also found that at 142 GHz, the indoor and outdoor sites have median ranks of 3.0 and 1.7 for the small-antenna case, and 4.9 and 2.4 for the large-antenna case assuming a rank threshold of 20 dB. The indoor site has a rank higher by 1.8 than the outdoor site, regardless of the antenna size. The rank decreases by only 20% and 15% for indoor and outdoor scenarios when the beam density is halved, allowing a significant reduction in implementation complexity of the beamspace MIMO without remarkably reducing the rank.**

***Index Terms*—Beamspace, multiple-input–multiple-output (MIMO), propagation, spatial multiplexing, subterahertz.**

I. Introduction

THE use of a sub-Terahertz (sub-THz) frequency band has been one of the research hotspots for future general cellular networks due to their capability of short-range superhigh-data-rate communications [2]. It is commonly thought that sub-THz radio links require directive beams at both link ends using a phased antenna array or radio lenses. Directive beams, especially in non-line-of-sight (NLOS) links, are essential to compensate for the high propagation loss, i.e., diffraction and scattering. Furthermore, directive antennas at both link ends allow spatial multiplexing through LOS connection and reflections on flat, smooth surfaces when available. Seminal works [3], [4], [5] indicate that there is more than one independent beam and multiple spatial clusters leading to the possibility of spatial multiplexing in sub-THz channels. Capacity improvement of *element-space* sub-THz multiple-input–multiple-output (MIMO) radio links was reported in [3] where the number of antenna elements in an array is identical to the number of transceiver chains. However, since the rank of sub-THz MIMO channels remains much less than the number of antenna elements, it would be more practical to consider a MIMO architecture with fewer fully equipped radio transceiver chains (digital signal processing paths, converters, and mixers). One such architecture is the *beamspace* MIMO, which can have a much smaller number of transceiver chains than the number of antennas in an array, as illustrated in Fig. 1. The multiple narrow high-gain beams are produced through an analog phase-shifting network [6], [7] and/or an antenna-array-fed lens [6], [8], [9].

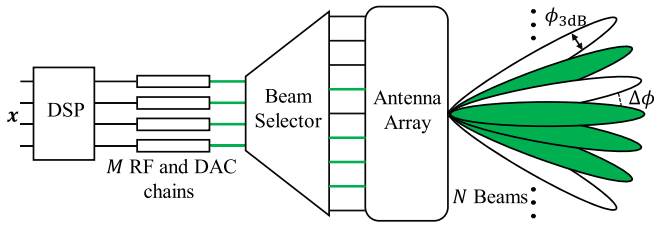

Fig. 1. Beamspace MIMO involves a phased antenna array at a link end, where an analog phase-shifting network and/or an antenna-array-fed lens form narrow high-gain beams across angles.

We evaluated the beamspace MIMO link using double-directional channel data derived from measurements [1]. The single-directional multipath data are first obtained through measurement campaigns in four different environments. We then applied a measurement-based ray-launcher (MBRL) to estimate the double-directional multipath data. To the best of our knowledge, this is the first paper to investigate the benefits of spatial multiplexing of beamspace MIMO links using measurement-derived double-directional sub-THz channels. Furthermore, the effects of varying configurations, e.g., antenna array size, beam density, and rank threshold, on channel rank are evaluated. In this letter, we show that the channel rank at 142 GHz channels is almost similar to that at 60 GHz channels [10] but significantly lower than at 5 GHz channels [11], [12].

Manuscript received 4 September 2023; revised 6 October 2023; accepted 11 October 2023. Date of publication 13 October 2023; date of current version 5 January 2024. This work was supported by the European Union's Horizon 2020 research and innovation programme within Project Hexa-X under Grant 101015956; and in part by the Smart Networks and Services Joint Undertaking through the European Union's Horizon Europe Research and Innovation Programme Hexa-X-II under Grant 101095759. The work of M. F. De Guzman was supported by the Department of Science and Technology, Science Education Institute of the Philippines. *(Corresponding author: Mar Francis De Guzman.)*

Mar Francis De Guzman is with the Department of Electronics and Nanoengineering, Aalto University, 02150 Espoo, Finland, and also with the Department of Science and Technology, Advanced Science and Technology Institute, Quezon, Philippines (e-mail: francis.deguzman@aalto.fi).

Nuutti Tervo is with the Centre for Wireless Communications, University of Oulu, 90570 Oulu, Finland (e-mail: nuutti.tervo@oulu.fi).

Pekka Kyösti is with the Centre for Wireless Communications, University of Oulu, 90570 Oulu, Finland, and also with Keysight Technologies Finland Oy, 90620 Oulu, Finland (e-mail: pekka.kyosti@oulu.fi).

Katsuyuki Haneda is with the Department of Electronics and Nanoengineering, Aalto University, 02150 Espoo, Finland (e-mail: katsuyuki.haneda@aalto.fi).

Digital Object Identifier 10.1109/LAWP.2023.3324614

II. Beamspace MIMO

A. System Model

A narrowband beamspace single-user MIMO system can be represented as

$$\mathbf{y} = \tilde{\mathbf{H}}\mathbf{x} + \mathbf{n} \tag{1}$$

where $\mathbf{y}$ is the received signal vector, $\tilde{\mathbf{H}}$ is an $N_{\mathrm{R}} \times N_{\mathrm{T}}$ beamspace channel matrix, $\mathbf{x}$ is the input signal vector, and $\mathbf{n}$ is a received complex Gaussian white noise vector with a power of N_0. N_{T} and N_{R} are the number of transmit and receive beams, respectively.

The double-directional propagation channel of a link is represented here as a set of discrete P multipath components (MPCs) as

$$\mathcal{P} = \{\alpha_p, \mathbf{\Omega}_p, \hat{\mathbf{\Omega}}_p, \tau_p\}_{p=1}^{P} \tag{2}$$

where α_p is the complex amplitude, $\mathbf{\Omega}_p = [\phi, \theta]$ is a vector of azimuth and polar angles on the Tx side while $\hat{\mathbf{\Omega}}_p = [\hat{\phi}, \hat{\theta}]$ is on the Rx side, and τ_p is the propagation delay of the pth path. These multipath parameters are derived from single-directional channel measurements complemented by an MBRL, as discussed in Section III. The amplitude and angular information of each path, i.e., (2), are then used to calculate the entries of the kth row and lth column of the beamspace channel matrix of a link as

$$\tilde{h}_{k,l} = \sum_{p=1}^{N_p} \alpha_p \sqrt{A_l(\mathbf{\Omega}_p) A_k(\hat{\mathbf{\Omega}}_p)} e^{\mathrm{j}\xi_p} \tag{3}$$

where $l = 1, 2, \ldots, N_{\mathrm{T}}$ and $k = 1, 2, \ldots, N_{\mathrm{R}}$ are indices representing the Tx and Rx beam pointing angles, and A is a beam gain pattern whose magnitude for pth path depends on the pointing angle of its main lobe and path's departure and arrival angles; ξ_p is a random phase of $[0, 2\pi)$ assigned to each path to represent small-scale fading. Note that the path delay from (2) is not included in generating the channel matrix; this study assumes a narrowband system. M_{T} and M_{R} baseband chains are available at Tx and Rx, respectively. The beam selector on each side chooses $M_{\mathrm{T/R}}$ beams with the highest powers, which are found by

$$\tilde{P}_k = \sum_{l=1}^{N_{\mathrm{T}}} |\tilde{h}_{k,l}|^2, \quad \tilde{P}_l = \sum_{k=1}^{N_{\mathrm{R}}} |\tilde{h}_{k,l}|^2 \tag{4}$$

then the resulting beamspace channel matrix $\mathbf{H}$ with the selected beams is given by entries

$$h_{m,n} = \{\tilde{h}_{k,l} | k \in \mathcal{K}, l \in \mathcal{L}\} \tag{5}$$

where $\mathcal{K}$ and $\mathcal{L}$, respectively, are sets of rows and columns providing M_{R} and M_{T} strongest beams at the Rx and Tx.

B. Beam Pattern

We consider here a uniform circular array (UCA) both in Tx and Rx. The antenna elements are Hertzian dipoles oriented on the z-axis and are arranged uniformly on the xy-plane with element spacing of $\lambda/2$, where λ is the signal wavelength. For a number of antenna elements Q, the radius of UCA is $r = \lambda/(4\sin(\pi/Q))$. The number of discrete beam directions is set to

$$N = \left\lfloor \frac{2\pi\beta}{\phi_{3\mathrm{dB}}} \right\rceil \tag{6}$$

where $\lfloor\cdot\rceil$ is the round operator, β is the beam density coefficient, and $\phi_{3\mathrm{dB}}$ is the azimuth half-power beamwidth (HPBW). The N beams are uniformly allocated around the horizontal plane with an azimuth step between adjacent beams given by

$$\Delta\phi = 2\pi/N. \tag{7}$$

Substituting (6) into (7) gives $\Delta\phi \approx \phi_{3\mathrm{dB}}/\beta$. When $\beta = 1$, the overall radiation pattern, i.e., combined radiation pattern of all the beams, has a gain flatness of about 3 dB. Meanwhile, $\beta < 1$ and $\beta > 1$, respectively, mean sparser and denser beams. In terms of implementation complexity, higher β translates to a greater number of required discrete beams, which is equivalent to a larger discrete Fourier transform matrix for the conventional phased array architecture [6], [7], or more antenna elements if an antenna-array-fed lens is used [6].

C. Capacity and Rank

Singular value decomposition is applied to the beamspace channel matrix $\mathbf{H} = \mathbf{U}\mathbf{\Sigma}\mathbf{V}^H$, where $\mathbf{U}^H$ and $\mathbf{V}$ are the decoding and precoding matrices, respectively, and $\{\cdot\}^H$ is the Hermitian transpose operator. The capacity of a single-user beamspace MIMO system with spatial multiplexing can then be calculated as

$$C = \sum_{i=1}^{K'} \log_2\left(1 + \frac{P_i}{N_0} s_i^2\right) \tag{8}$$

where K' is the rank of the beamspace channel matrix, P_i is the power allocated, and s_i is the singular value at ith substream. Note that s_i is a nonnegative real number. Assuming that there is a perfect channel state information available at Tx, the capacity can be maximized through water-filling power allocation of the Tx power P_{T} as

$$P_i = \max\left(\mu' - \frac{N_0}{s_i^2}, 0\right) \tag{9}$$

where μ' is selected to satisfy the power constraint $P_{\mathrm{T}} = \sum_{i=1}^{K} P_i$, and P_{T} is the total Tx power fed to the antenna elements.

For each link, L random channel realizations are generated where each realization has a unique set of random phases ξ_p applied to the channel coefficients as indicated in (3). The ergodic capacity $\bar{C}$ of each link is then calculated by taking the average of the instantaneous capacity C across L channel realizations. The resulting rank $\tilde{K}$ of these L realizations of the complete beamspace channel matrix $\tilde{\mathbf{H}}$ is calculated as

$$\tilde{K} = \min\left(\mathrm{rank}\left(\mathbf{R}_{\mathrm{T}}\right), \mathrm{rank}\left(\mathbf{R}_{\mathrm{R}}\right)\right) \tag{10}$$

where $\mathbf{R}_{\mathrm{T}}$ and $\mathbf{R}_{\mathrm{R}}$, respectively, are the Tx and Rx covariance matrices calculated as $\mathbf{R}_{\mathrm{T}} = \mathbb{E}[\tilde{\mathbf{H}}^H\tilde{\mathbf{H}}]$ and $\mathbf{R}_{\mathrm{R}} = \mathbb{E}[\tilde{\mathbf{H}}\tilde{\mathbf{H}}^H]$ where $\mathbb{E}[\cdot]$ is the expectation operator. The rank is defined here

TABLE I
MEASUREMENT CAMPAIGN DETAILS

Environment	Number of LOS links	Number of NLOS links	Link distance range (m)
Entrance hall	28	47	3-65
Suburban	35	4	2-162
Residential	23	38	20-175
City Center	12	23	10-178

as the number of singular values within a threshold from the strongest singular value.

III. DOUBLE-DIRECTIONAL MULTIPATH DATA

Measurements of radio channels were conducted in an entrance hall and three outdoor environments, such as suburban, residential, and city center. A number of LOS and NLOS links and link distance ranges are summarized in Table I. A channel sounder based on a vector network analyzer integrated with frequency converters is employed. It measures from 140 to 144 GHz resulting in a delay resolution of 0.25 ns. The Tx and Rx are equipped with an omnidirectional and rotator-mounted directional horn antenna with 10° azimuth HPBW, respectively. The azimuth on the Rx side is scanned with a 5° step while keeping the antenna's main beam fixed in the horizontal plane. The channel sounder and measurements are further described in [13] and [14]. The single-directional power-angular delay profile (PADP) contains the received signal intensity as a function of the propagation delay and the horn's broadside direction is obtained from these measurements. To determine the gain contributed by the wave propagation alone, the Tx and Rx antenna gains and the shape of radiation patterns were de-embedded from the PADP, leading to the discrete multipath parameters [15], [16].

The resulting single-directional multipath data are then mapped to the environment's detailed geometry, in the form of a point cloud, to estimate the path trajectory using an MBRL [14]. This ray-based simulation method launches rays from the receiver in the directions where the measured MPCs are observed, and the measured propagation delay defines their length. The trajectory of each launched ray that ends up close to the transmitter is considered the estimated trajectory of the corresponding measured multipath. The double-directional path data as in (2) and their interaction point(s) on the physical environment are then derived from this estimated trajectory. Up to fourth-order reflections are allowed using the MBRL.

About 10% of the multipaths were not successfully mapped onto the geometry due to the limitations of the tool and the input data. The angles of these unmapped paths are determined by randomly drawing values from the best-fitting distribution observed in the mapped paths. The Laplace distribution is a good fit for the angular information we obtained regardless of the environment and link type. The Laplace probability density function is described by the mean of the distribution, which is equal to the direction of Rx seen from Tx, and by the scale parameter b, which varies with the environments and link types as listed in Table II. A random azimuth angle-of-departure is then generated by

$$\hat{\phi}_{\mathrm{T}} = \Phi + \phi_{\mathrm{TR}} \tag{11}$$

TABLE II
LAPLACIAN SCALE PARAMETER

Link Type	Entrance Hall	Suburban	Residential	City Center
LOS	17.7	3.8	7.2	11.9
NLOS	47.3	71.9	55.1	45.6

TABLE III
UCA SPECIFICATIONS

Configuration	r (λ)	r (mm)	Q	N	$\phi_{3\mathrm{dB}}$ (°)	Gain (dBi)
C_1	1.3	2.7	16	23	16	13
C_2	5.1	10.8	64	90	4	19
C_3	10.2	21.5	128	180	2	22
C_4	20.4	43.0	256	360	1	25

where Φ is a random value with Laplacian distribution, i.e., $\Phi \sim \mathcal{L}_{\mathrm{d}}(0, b)$, and ϕ_{TR} is the direction of Rx seen from Tx. Additional comparisons between the LOS and NLOS channels in terms of the path loss model, delay, and angular dispersions in all four environments can be found in [2, Sec. 6.2.1].

IV. RESULTS AND DISCUSSION

A center frequency of 142 GHz, transmit power of 20 dBm, and 100 channel realizations are assumed in the simulations. The noise power per beam is calculated as $N_0 = kTB$, where k is the Boltzmann constant, T is the ambient temperature, and B is the system bandwidth. Assuming a temperature and bandwidth of 290 K and 1 GHz, the noise power is -84 dBm. The UCA configurations C_1, C_2, C_3, and C_4 considered in the simulations are summarized in Table III. Each configuration has a different antenna size, resulting in varying HPBW and gain. We assume a downlink transmission scenario, where the base station serves as the Tx and the user equipment acts as the Rx. The Tx is set to have a larger antenna size than the Rx. In the following simulations, the configurations C_2 and C_1 for the Tx and Rx, a beam density of 1, and a rank threshold of 20 dB are assumed unless otherwise stated. The C_2–C_1 and C_4–C_2 configuration pairs are considered as the small and large antenna cases. The synthesized beam patterns with the mentioned UCA setup in Section II-B have a sidelobe level of 8 dB lower than the main lobe regardless of the antenna size, and no sidelobe suppression is applied. The rank presented in the following results corresponds to the rank $\tilde{K}$ as defined in (10). In addition, the indoor site refers to the entrance hall environment, and the outdoor site refers to the combined results of those mentioned in Section III.

A. Capacity and Rank

The ergodic capacity using single-stream ($M = 1$) and multistream ($M = 8$) transmissions, and rank for both sites are shown in Fig. 2. The single-stream transmission is equivalent to beamforming where its capacity is calculated as $C_s = \log_2(1 + \frac{P_{\mathrm{T}}}{N_0}|h|^2)$, where h is the highest channel coefficient obtained using (5). Meanwhile, multistream corresponds to spatial multiplexing where the capacity is calculated using (8). Fig. 2 shows that there is a significant capacity gain for both sites, especially for the indoor case, by using 8×8 multistream beamspace MIMO compared to a single stream. The average capacity gain

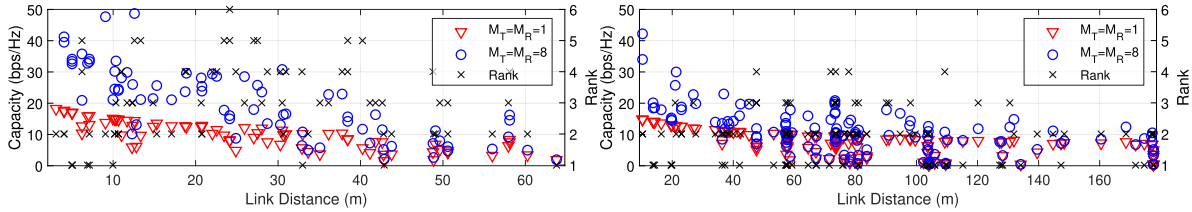

Fig. 2. Ergodic capacity of each link using single-stream ($M_{\mathrm{T/R}} = 1$) and multistream ($M_{\mathrm{T/R}} = 8$) beamspace MIMO, and beamspace rank in (a) indoor and (b) outdoor scenarios. The total Tx power is set to 20 dBm, the noise floor is set to -84 dBm, and the rank threshold is set to 20 dB.

TABLE IV
RANK AT DIFFERENT FREQUENCIES AND ENVIRONMENTS

Frequency	5 GHz		60 GHz		142 GHz	
Scenario	Office	Street	Lobby	Street	Entrance hall	Outdoor
Med. rank	7.5	7.0	1.5	1.5	3.0	1.7
Ref.	[12]	[11]	[10]	[10]	This study	This study

TABLE V
RANK UNDER DIFFERENT ANTENNA SPECIFICATIONS

Tx UCA rad. (λ)	**Rx UCA rad.** (λ)	**Med. rank**	
		Indoor	Outdoor
5.1	1.3	3.0	1.7
10.2	1.3	3.4	1.9
20.4	1.3	3.6	2.0
20.4	5.1	4.9	2.4

Beam density	**Med. rank**	
	Indoor	Outdoor
1	3.1	1.7
1/2	2.3	1.5
1/4	1.8	1.2
1/8	1.4	1.0

of the links with link distance below 60 m is 200% for the indoor case and 150% for the outdoor case.

The 8×8 beamspace MIMO channel shows a median (med.) rank of 3.0 and 1.7 for the indoor and outdoor environments. These results are comparable with 60 GHz channels and significantly lower than 5 GHz channels as summarized in Table IV. The rank estimates for the 60 GHz and the street scenario at 5 GHz are approximated from [10, Fig. 2(e)] and [11, Fig. 2], respectively. The lower rank in the outdoor site compared to the indoor site, as observed in Fig. 2 for our 142 GHz measurements, can be explained by the indoor site having walls on all sides and ceilings, generating MPCs in more directions than the outdoor site. For both environments, the rank itself does not strongly vary with the link distance while the capacity decreases due to the reduced SNR.

B. Varying Antenna Size, Beam Density, and Threshold

The median rank across all the links under different Tx and Rx antenna sizes, given in terms of UCA radius $r_{\mathrm{T/R}}$ in λ are summarized in Table V. The corresponding UCA specifications are listed in Table III. For both environments, the rank increases as the antenna size increases due to the decrease in beamwidth and increase in SNR. Increasing the Tx size, while the Rx size is fixed, shows a limited rank improvement as the Rx's relatively wide beamwidth limits its capability to resolve. The subsequent increase of Rx antenna size to 5.1λ shows a significant increase in rank. The median rank for the large antenna case is 4.9 and 2.4 for the indoor and outdoor sites. In all cases, the rank is approximately higher by 1.8 in our indoor site than the outdoor site.

The rank under different beam densities is listed in Table V. Reducing the beam density by 50% results only in a 20% decrease in rank for the indoor case and a 15% decrease for the outdoor case. Fig. 3 shows the median and quartiles of the rank under different thresholds. The rank in the indoor site increases and disperses more with the increasing threshold than in the outdoor site. Using a higher rank threshold than the typical 20 dB reveals the presence of weak spatial clusters, especially in the indoor site.

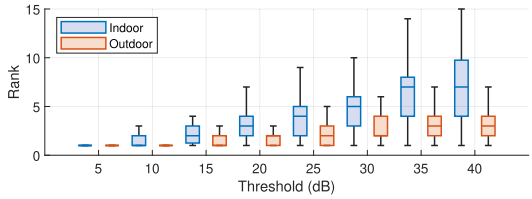

Fig. 3. Rank under varying thresholds with Tx and Rx UCA radii of 5.1λ and 1.3λ. The box's bottom, middle, and top lines represent the first, second (median), and third quartiles, respectively.

V. CONCLUSION

In this letter, we evaluated the capacity and rank of the beamspace MIMO channels using double-directional multipath estimates in indoor and outdoor scenarios at 142 GHz. The capacity gain at link distances below 60 m is 200% and 150% for the indoor and outdoor when spatial multiplexing with Tx and Rx UCA radii of 5.1λ and 1.3λ is employed. The rank varies randomly while the capacity gain decreases with link distance due to the fixed total transmit power we assumed in the study. The rank at 142 GHz channels is also found comparable to that at 60 GHz channels and significantly lower than at 5 GHz channels reported in the literature. The median ranks for indoor and outdoor sites are 3.0 and 1.7 for the small antenna case, and 4.9 and 2.4 for the large antenna case assuming a rank threshold of 20 dB. The indoor site has a rank about twice as high as the outdoor site regardless of the antenna size. The rank decreases only by 20% for the indoor case and 15% for the outdoor case when the beam density is halved. This means that implementation complexity can be reduced without reducing the rank noticeably.

ACKNOWLEDGMENT

The double-directional sub-THz channel model [1] used in this work was developed under the European Union's Horizon 2020 research and innovation programme project Hexa-X. The work that analyzes the MIMO channel characteristics was supported by the Smart Networks and Services Joint Undertaking under the European Union's Horizon Europe research and innovation programme Hexa-X-II.

REFERENCES

[1] M. F. de Guzman, K. Haneda, and P. Kyösti, "Measurement-based MIMO channel model at 140 GHz," 2023, version 1, doi: 10.5281/zenodo.7640352.

[2] A. Nimr, Ed., "Deliverable D2.3 radio models and enabling techniques towards ultra-high data rate links and capacity in 6G," Hexa-X project, 2023. [Online]. Available: https://hexa-x.eu/deliverables/

[3] S. Ju and T. S. Rappaport, "Sub-terahertz spatial statistical MIMO channel model for urban microcells at 142 GHz," in *Proc. IEEE Glob. Commun. Conf.*, 2021, pp. 1–6.

[4] P. Kyösti, M. F. De Guzman, K. Haneda, N. Tervo, and A. Pärssinen, "How many beams does sub-THz channel support?," *IEEE Antennas Wireless Propag. Lett.*, vol. 21, no. 1, pp. 74–78, Jan. 2022.

[5] Y. Xing, T. S. Rappaport, and A. Ghosh, "Millimeter wave and sub-THz indoor radio propagation channel measurements, models, and comparisons in an office environment," *IEEE Commun. Lett.*, vol. 25, no. 10, pp. 3151–3155, Oct. 2021.

[6] J. Brady, N. Behdad, and A. M. Sayeed, "Beamspace MIMO for millimeter-wave communications: System architecture, modeling, analysis, and measurements," *IEEE Trans. Antennas Propag.*, vol. 61, no. 7, pp. 3814–3827, Jul. 2013.

[7] A. Molisch and X. Zhang, "FFT-based hybrid antenna selection schemes for spatially correlated MIMO channels," *IEEE Commun. Lett.*, vol. 8, no. 1, pp. 36–38, Jan. 2004.

[8] J. Ala-Laurinaho et al., "2-D beam-steerable integrated lens antenna system for 5G e-band access and backhaul," *IEEE Trans. Microw. Theory Techn.*, vol. 64, no. 7, pp. 2244–2255, Jul. 2016.

[9] X. Gao, L. Dai, S. Zhou, A. M. Sayeed, and L. Hanzo, "Wideband beamspace channel estimation for millimeter-wave MIMO systems relying on lens antenna arrays," *IEEE Trans. Signal Process.*, vol. 67, no. 18, pp. 4809–4824, Sep. 2019.

[10] W. Sloane, C. Gentile, M. Shafi, J. Senic, P. A. Martin, and G. K. Woodward, "Measurement-based analysis of millimeter-wave channel sparsity," *IEEE Antennas Wireless Propag. Lett.*, vol. 22, no. 4, pp. 784–788, Apr. 2023.

[11] R. He, B. Ai, G. Wang, M. Yang, C. Huang, and Z. Zhong, "Wireless channel sparsity: Measurement, analysis, and exploitation in estimation," *IEEE Wireless Commun.*, vol. 28, no. 4, pp. 113–119, Aug. 2021.

[12] M. Matthaiou, A. M. Sayeed, and J. A. Nossek, "Sparse multipath MIMO channels: Performance implications based on measurement data," in *Proc. IEEE 10th Workshop Signal Process. Adv. Wireless Commun.*, 2009, pp. 364–368.

[13] M. F. De Guzman, M. Hassan, and K. Haneda, "Uncertainty of millimeter-wave channel sounder due to integration of frequency converters," in *Proc. 17th Int. Symp. Wireless Commun. Syst.*, 2021, pp. 1–6.

[14] M. F. De Guzman, P. Koivumäki, and K. Haneda, "Double-directional multipath data at 140 GHz derived from measurement-based ray-launcher," in *Proc. IEEE 95th Veh. Technol. Conf.*, 2022, pp. 1–6.

[15] K. Haneda, S. L. H. Nguyen, J. Järveläinen, and J. Putkonen, "Estimating the omni-directional pathloss from directional channel sounding," in *Proc. 10th Eur. Conf. Antennas Propag.*, 2016, pp. 1–5.

[16] S. L. H. Nguyen, K. Haneda, and J. Putkonen, "Dual-band multipath cluster analysis of small-cell backhaul channels in an urban street environment," in *Proc. IEEE Globecom Workshops*, 2016, pp. 1–6.